Supporting Information

Zhong et al. 10.1073/pnas.1317173111

SI Materials and Methods

Thermal Denaturation. Melting curves of 10–15 μM protein were recorded in the UV (222 nm) and visible (434 nm) regions in 1- and 4-mm quartz cuvettes, respectively. The temperature range of each scan was 20–90 °C (293–363 K). Ferric samples were dissolved in freshly prepared and degassed 100 mM buffered solutions before each measurement. Ferrous samples were prepared in a glove box by dithionite reduction of the heme iron and subsequent run of the protein solution on a desalting column. A small excess of dithionite (~25 μM) was incorporated into each ferrous sample to ensure reducing conditions throughout the scan. Samples were transferred to sealed cuvettes in the glove box, and the oxidation state of the protein was confirmed before and after each experiment with absorption spectra. Thermodynamic parameters were extracted through nonlinear curve fitting of the CD signals to Eq. **S1** using the MATLAB curve-fitting tool (MathWorks):

$$\text{ellipticity}(T) = \frac{\left[(m_f T + b_f) + (m_u T + b_u)\right]\exp\left[\left(-\frac{\Delta H_{D,vH}}{R}\right)\left(\frac{1}{T}-\frac{1}{T_m}\right)\right]}{1+\exp\left[\left(-\frac{\Delta H_{D,vH}}{R}\right)\left(\frac{1}{T}-\frac{1}{T_m}\right)\right]}, \quad \textbf{[S1]}$$

where m_f, b_f, and m_u, b_u are the slopes and y intercepts of the pretransitional (low-temperature, folded protein) and posttransitional (high-temperature, unfolded protein) regions of the melting curve; R is the gas constant; T_m and $\Delta H_{D,vH}$ are the midpoint of the unfolding transition and the van't Hoff enthalpy of denaturation at T_m, respectively.

The free-energy analysis was carried out as previously described (1, 2). The values of ΔC_p, the unfolding heat capacity, were determined by linear least-squares fitting of $\Delta H_{D,vH}$ dependences versus T_m over a pH range of 3.5–5.5. The enthalpy ΔH_D and the entropy ΔS_D of denaturation at a reference temperature T_{REF} were calculated using Eqs. **S2** and **S3**, respectively, as follows:

$$\Delta H_D = \Delta H_{D,vH} + \Delta C_p (T_{REF} - T_m), \quad \textbf{[S2]}$$

$$\Delta S_D = \frac{\Delta H_{D,vH}}{T_m} + \Delta C_p \ln\left(\frac{T_{REF}}{T_m}\right). \quad \textbf{[S3]}$$

The differences in the free energy of unfolding between ferrous and ferric variants ($\Delta\Delta G_{D,\ II\text{-}III}$) were compared with the values from electrochemical measurements (Table 1); Eq. **S4** relates $\Delta\Delta G_{D,\ II\text{-}III}$ to the midpoint potentials (3):

$$\Delta\Delta G_{D,\ II-III} = -nF(E^\circ_D - E^\circ_N). \quad \textbf{[S4]}$$

In Eq. **S4**, n is the number of electrons transferred, F is the Faraday constant, and E^o are the formal potentials for the native (Table 1) and denatured proteins (−150 mV) (4).

Determination of the pK_a for the Alkaline Transition. A protein solution (12 mL) at a concentration between 7 and 14 μM was titrated with micromolar additions of acid (1 M HCl) or base (1 M NaOH) to sample the pH range between 7 and 13. Changes in the heme absorption at each addition of acid (or base) were monitored on a Shimadzu UV-1201 UV-vis spectrometer. All experiments were carried out in a glove box under a nitrogen atmosphere. Ferric and ferrous samples were prepared in a thoroughly degassed 100 mM sodium phosphate buffer; ferrous samples had added dithionite at concentration of ~35 μM. The pK_a values of the transitions were extracted through nonlinear curve fitting of measured absorbance values A to Eq. **S5**:

$$A = \frac{(A_{acid} + A_{alk} \times 10^{n(pK_a(obs)-pH)})}{(1+10^{n(pK_a(obs)-pH)})}, \quad \textbf{[S5]}$$

where A_{acid} and A_{alk} are the absorbance values for the beginning (acidic) and ending (alkaline) regions of the curve and n is the number of protons.

Binding of *N*-Acetyl Cysteine to Microperoxidase-8. Solutions of microperoxidase-8 (MP8) and *N*-acetylcysteine (AcCys) (Fisher) in a deoxygenated 100 mM sodium phosphate buffer at pH 7.4 were prepared under a nitrogen atmosphere. A solution of MP8 was transferred to a quartz cuvette, which was sealed with a rubber septum. A stir bar was also placed into the cuvette to ensure complete solution mixing. A concentrated solution of AcCys was taken up with a 500-μL gastight Hamilton syringe and inserted into the cuvette before removal from the glove box. An atmosphere of argon was maintained inside the cuvette by adding an argon-containing balloon also inserted through the septum. Additionally, an oxygen-scavenging solution composed of 0.5 μM glucose oxidase, 0.05 μM catalase, and 0.03 mg glucose was added to the AcCys and MP8 solutions. Titrations were carried out through controlled additions of AcCys through the syringe. Samples were equilibrated for at least 5 min before each measurement. Titration data were fit to Eq. **S6** (5), where $[MP8]_0$ and $[L]_0$ were the concentrations of AcMP8 and added AcCys:

$$\Delta A = \frac{\Delta A_{max}}{2K[MP8]_0}\left\{1 + K[MP8]_0 + K[L]_0 - \left((1+K[MP8]_0+K[L]_0)^2 - 4K^2[MP8]_0[MP8]_0\right)^{1/2}\right\}. \quad \textbf{[S6]}$$

Kinetics of Redox Reactions. The compounds $Ru(NH_3)_6Cl_3$ (Strem) and sodium dithionite (MCB) were used as received. The cobalt complex $Co(phen)_3Cl_3$ was synthesized from $[Co(NH_3)_5Cl]Cl_2$ (Alfa Aesar) and 1,10-phenanthroline (Sigma-Aldrich) according to the published procedure (6). Concentrations of $Co(phen)_3^{3+}$ in working solutions were determined spectrophotometrically (7). The Eu^{2+}-EGTA complex was prepared by mixing europium (II) chloride ($EuCl_2$) (Sigma-Aldrich) and EGTA (Sigma-Aldrich) in a buffer. The concentration of Eu^{2+}-EGTA complex was determined by electronic absorption spectra ($\varepsilon_{330\ nm}$ = 700 $M^{-1}\cdot cm^{-1}$) (8).

Before each stopped-flow measurement, the instrument lines were flushed with dithionite to remove trace amounts of oxygen, and all samples were prepared under nitrogen. Mixing sequences were based on three syringes that contained deoxygenated buffer, oxidants [$Co(phen)_3^{3+}$ or $Ru(NH_3)_6^{3+}$] or reductants (dithionite or Eu^{2+}-EGTA), and protein, respectively. The final concentration of protein was around 5 μM. The final concentrations of dithionite and Eu^{2+}-EGTA were between 1.7 and 8.3 mM and between 0.1 to 1.0 mM, respectively. Traces were collected using

the BioKine program (BioLogic) and analyzed using SFit (BioLogic), Origin Pro-8 SR0 (OriginLab), or Sigma Plot 10.0 (Systat Software).

In the measurements of slow kinetics (the second step of oxidation reactions), the spectra were recorded every 1 s for 15 min or until the reaction reached equilibrium. In the study of the deuterium effects on the reaction rates, the concentrated protein was reduced by dithionite, then diluted fivefold with D_2O and aged for at least 10 min before loading onto the desalting column, which was equilibrated with a 100 mM sodium phosphate buffer in D_2O. In the studies of the glycerol effect, the ferrous protein collected from the desalting column was diluted with a 100 mM sodium phosphate buffer containing high concentration of glycerol at pH 7.4 to reach the desired concentration of the additive. The kinetics was analyzed using Origin Pro-8 SR0 or Sigma Plot 10.0.

1. Cohen DS, Pielak GJ (1995) Entropic stabilization of cytochrome *c* upon reduction. *J Am Chem Soc* 117(6):1675–1677.
2. Liggins JR, Lo TP, Brayer GD, Nall BT (1999) Thermal stability of hydrophobic heme pocket variants of oxidized cytochrome *c*. *Protein Sci* 8(12):2645–2654.
3. Pascher T, Chesick JP, Winkler JR, Gray HB (1996) Protein folding triggered by electron transfer. *Science* 271(5255):1558–1560.
4. Bixler J, Bakker G, McLendon G (1992) Electrochemical probes of protein folding. *J Am Chem Soc* 114:6938–6939.
5. Wendt H, et al. (1997) Very rapid, ionic strength-dependent association and folding of a heterodimeric leucine zipper. *Biochemistry* 36(1):204–213.
6. Maki N (1969) Methods of preparing the 2,2′-dipyridyl and 1,10-phenanthroline cobalt (III) complexes of the [CoX2dip2]- and [CoX2phen2]-type. *Bull Chem Soc Jpn* 42: 2275–2281.
7. Farina RD, Wilkins RG (1968) Electron-transfer rate studies of a number of cobalt-(II)-cobalt(III) systems. *Inorg Chem* 7(3):514–518.
8. Vincent KA, et al. (2003) Instantaneous, stoichiometric generation of powerfully reducing states of protein active sites using Eu(II) and polyaminocarboxylate ligands. *Chem Commun (Camb)* (20):2590–2591.

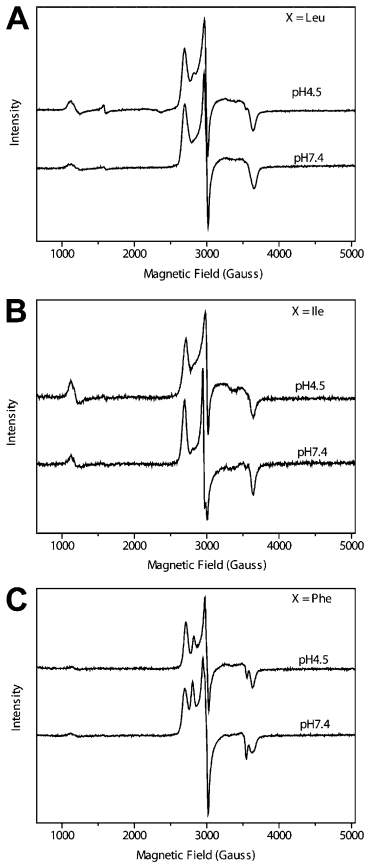

Fig. S1. EPR spectra at 10 K of ferric Thr78Cys/Lys79Gly/Met80X variants at pH 4.5 and 7.4: (*A*) X = Leu, (*B*) X = Ile, and (*C*) X = Phe.

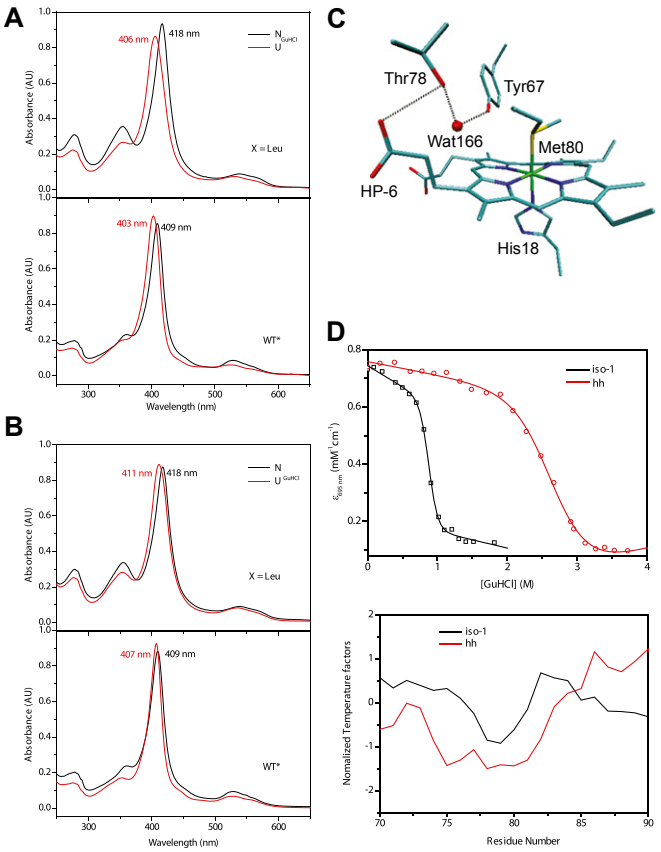

Fig. S2. Electronic absorption spectra of ferric Thr78Cys/Lys79Gly/Met80Leu and WT* iso-1 cyt *c* at pH 5.0 (*A*) and 7.4 (*B*) in a buffer (*Upper*) and with added 6.0 M GuHCl (*Lower*). (*C*) A hydrogen-bonding network involving Thr78. (*D*) Stability (*Upper*) with respect to GuHCl denaturation at pH 7.4 of the Met80 region in ferric yeast iso-1 (1) and horse heart cyt *c* (this work) monitored by absorption measurements at 695 nm. Temperature factors (*Lower*) for ferric yeast iso-1 cyt *c* [Protein Data Bank (PDB) entry 2YCC] (2) and horse heart cyt *c* (PDB entry 1HRC) (3) suggest greater mobility of the Met80 loop in the former protein.

1. Godbole S, Dong A, Garbin K, Bowler BE (1997) A lysine 73→histidine variant of yeast iso-1-cytochrome *c*: Evidence for a native-like intermediate in the unfolding pathway and implications for m value effects. *Biochemistry* 36(1):119–126.
2. Berghuis AM, Brayer GD (1992) Oxidation state-dependent conformational changes in cytochrome *c*. *J Mol Biol* 223(4):959–976.
3. Bushnell GW, Louie GV, Brayer GD (1990) High-resolution three-dimensional structure of horse heart cytochrome *c*. *J Mol Biol* 214(2):585–595.

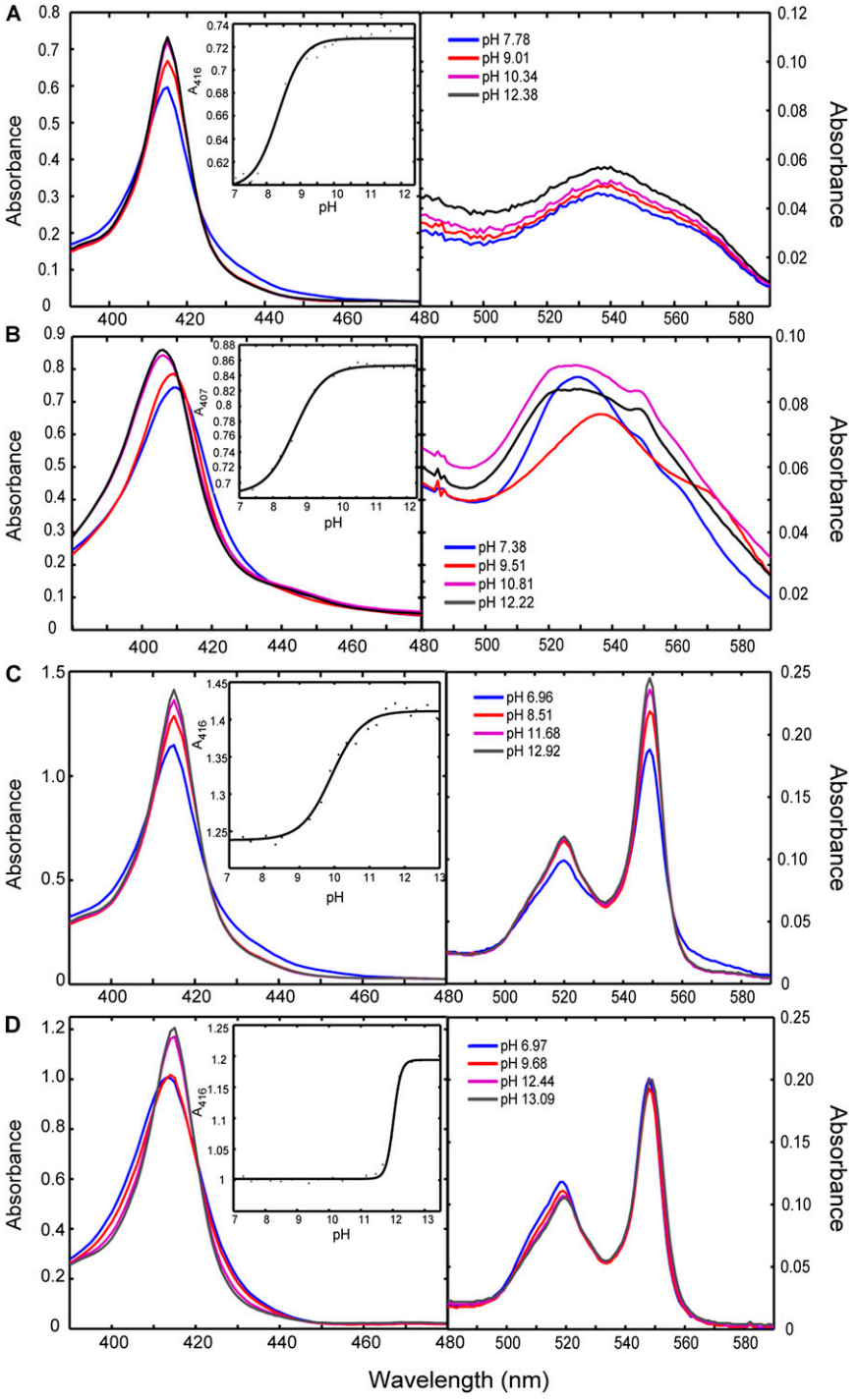

Fig. S3. Changes with pH in the Soret and Q-band regions of the absorption spectra for ferric Thr78Cys/Lys79Gly/Met80Leu (*A*) and WT* (*B*) as well as ferrous Thr78Cys/Lys79Gly/Met80Leu (*C*) and WT* (*D*). (*Insets*) Titration curves used to determine pK_a values listed in Table 1; lines are fits to Eq. **S5**.

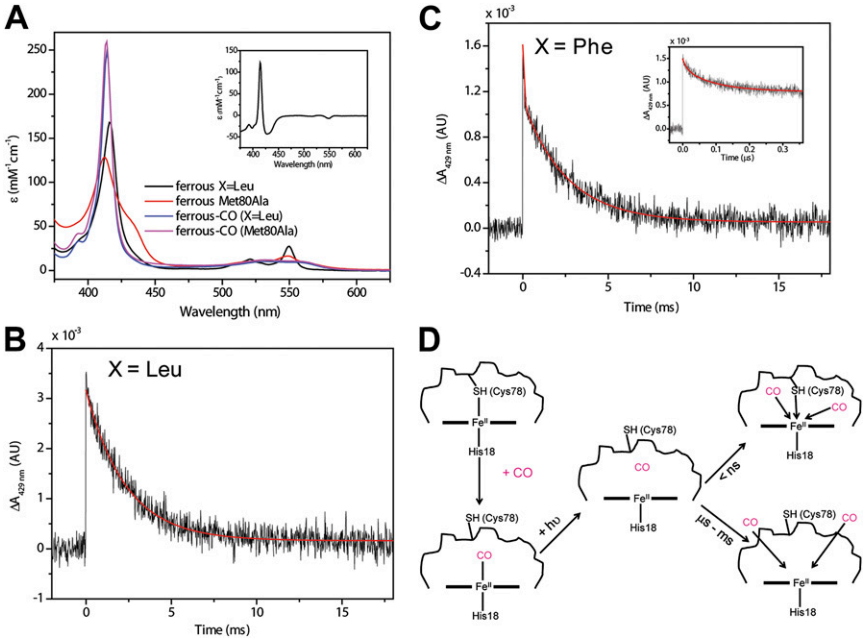

Fig. S4. (*A*) Electronic absorption spectra in a sodium phosphate buffer at pH 7.4 of ferrous yeast Met80Ala, Thr78Cys/Lys79Gly/Met80Leu, and their CO adducts. (*Inset*) The difference spectrum ferrous CO adduct minus ferrous protein in the absence of CO for Met80Ala (a variant that at pH 7.4 does not have a sixth endogenous ligand to coordinate to the heme). Photolysis transients for the Leu (*B*) and Phe (*C*) variants of Thr78Cys/Lys79Gly/Met80X cyt *c*. (*Inset*) The transient for the Phe variant on the shorter timescale showing fast CO-independent phase. (*D*) A cartoon illustrating processes during CO photolysis experiments.

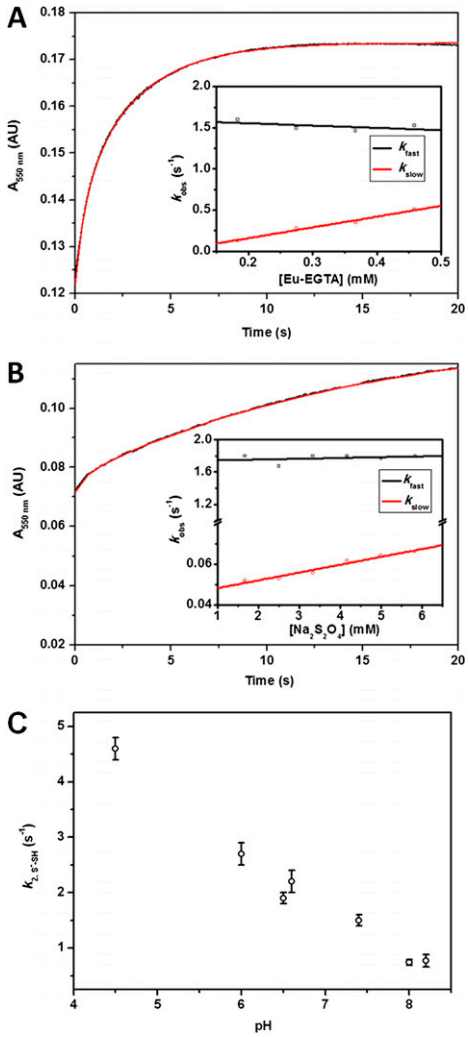

Fig. S5. Representative kinetic progress curve for reduction of ferric Thr78Cys/Lys79Gly/Met80Leu with (*A*) 0.36 mM Eu^{2+}-EGTA and (*B*) 5.8 mM sodium dithionite in a sodium phosphate buffer at pH 7.4. (*Insets*) Dependences of the observed constants k_{fast} and k_{slow} on concentrations of reductants. (*C*) pH dependence of the rate constant k_{fast} in reactions of ferric Thr78Cys/Lys79Gly/Met80Leu with Eu^{2+}-EGTA.

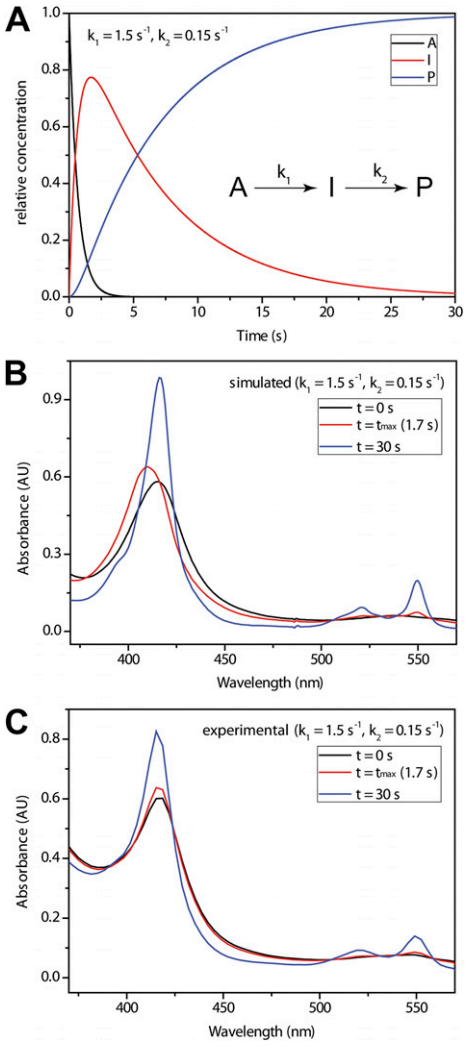

Fig. S6. (*A*) Simulations of kinetic progress curves for the route Red^A using experimentally measured rate constants k_1 and k_2. If the rate constants k_1 and k_2 were to correspond to $k_{3,\ S^-\text{-}SH}$ and $k_{ET,\ SH}$, respectively, the ferric thiol intermediate should be clearly visible (*B*), in disagreement with experimental results (*C*).

Table S1. Spectroscopic properties of Thr78Cys/Lys79Gly/Met80X variants of yeast iso-1 cyt *c* and AcCys adduct of AcMP8 at pH 7.4

Variant	λ_{max}, nm					EPR *g* values[a]		
	δ	Soret (γ)	β	α	Near-IR	g_z	g_y	g_x
				Ferric				
X = Leu	355.2	417.6	538.4		~630, 727.8	2.52	2.26	1.87
X = Ile	355.2	418.0	538.4		~630, 719.4	2.51	2.26	1.87
X = Phe	355.8	418.2	538.4		~630, 727.2	2.51; 2.42[b]	2.26[b]	1.86; 1.91[b]
AcMP8 + AcCys		417	538 (565 shoulder)		641, 767		n.d.[c]	
				Ferrous				
X = Leu		416.6	520.8	549.2				
X = Ile		416.4	520.8	549.4				
X = Phe		416.4	520.8	549.4				
AcMP8 + AcCys		416	520	550				

[a]From measurements at 10 K; spectra are shown in Fig. 1*B* and Fig. S1.
[b]Two sets of overlapping signals; see Fig. 1*B*.
[c]Not determined.

Table S2. Thermodynamic parameters for wild-type WT* and Thr78Cys/Lys79Gly/Met80X variants of yeast iso-1 cyt *c* from thermal denaturation experiments at pH 7.4

Variant	Ferric		Ferrous	
	T_m, K	$\Delta H_{D,vH}$, kcal/mol	T_m, K	$\Delta H_{D,vH}$, kcal/mol
WT*[a]	332.6 ± 0.5	88 ± 2	359.1 ± 0.6	130 ± 2
X = Leu	342.3 ± 0.5	52.5 ± 0.9	321.0 ± 0.5	44.9 ± 0.5
X = Ile	341.6 ± 0.4	51.6 ± 0.6	320.6 ± 0.5	44.5 ± 0.8
X = Phe	342.9 ± 0.4	54 ± 1	321.3 ± 0.4	45.2 ± 0.9

In a sodium phosphate buffer at pH 7.4; results at pH 5.0 are presented in Table 1.
[a]Contains two background mutations, Lys72Ala and Cys102Ser, to prevent Lys72 coordination to the heme and formation of cyt *c* dimers, respectively.

Table S3. Quantum yields for CO photodissociation, rate constants of CO rebinding to ferrous heme, and rate constants of electron transfer and protonation (deprotonation) in redox transformations of Thr78Cys/Lys79Gly/Met80X variants of yeast iso-1 cyt *c*

Variant	Quantum yield (φ)[a]	$k_{on,\ CO} \times 10^{-6}$, $M^{-1}{\cdot}s^{-1}$	$k_{-ET,\ SH} \times 10^{-5}$, $M^{-1}{\cdot}s^{-1}$[b]	$k_{3,\ SH\text{-}S^-}$, s^{-1}	$k_{slow} \times 10^{-3}$, $M^{-1}{\cdot}s^{-1}$[c]	k_{fast}, s^{-1}
X = Leu	0.021 ± 0.001	2.4 ± 0.1	2.2 ± 0.3	0.039 ± 0.004	1.3 ± 0.2	1.5 ± 0.1
X = Ile	0.022 ± 0.001	1.7 ± 0.1	2.1 ± 0.3	0.044 ± 0.005	1.5 ± 0.1	1.3 ± 0.1
X = Phe	0.028 ± 0.001	3.4 ± 0.2	3.1 ± 0.2	0.028 ± 0.002	0.3 ± 0.1	1.5 ± 0.2

At pH 7.4 in a 100 mM sodium phosphate buffer.
[a]The corresponding quantum yields of Met80Ala and Cmcyt *c* determined in the same set of measurements were 0.004 ± 0.001 and 0.21 ± 0.01, respectively, in accord with previous reports (1, 2).
[b]With $Ru(NH_3)_6^{3+}$ as an oxidant.
[c]With Eu^{2+}-EGTA as a reductant.

1. Silkstone G, Stanway G, Brzezinski P, Wilson MT (2002) Production and characterisation of Met80X mutants of yeast iso-1-cytochrome *c*: Spectral, photochemical and binding studies on the ferrous derivatives. *Biophys Chem* 98(1-2):65–77.
2. Bren KL, Gray HB (1993) Structurally engineered cytochromes with novel ligand-binding sites: Oxy and carbon monoxy derivatives of semisynthetic horse heart Ala80 cytochrome *c*. *J Am Chem Soc* 115(22):10382–10383.